14th International Symposium on Turbulence and Shear Flow Phenomena (TSFP14)
Heidelberg, Germany, July 28–31, 2026

INSIGHTS INTO THE NEAR-WALL VORTICITY DYNAMICS VIA DIRECT NUMERICAL SIMULATIONS OF CHANNEL FLOWS SUBJECTED TO IMPULSIVE RE_τ CHANGE

Anthony Settlemier
Department of Mechanical Engineering
The University of Akron
Akron OH 44325, USA
ams593@uakron.edu

Saikishan Suryanarayanan
Department of Mechanical Engineering
The University of Akron
Akron OH 44325, USA
ssuryanarayanan@uakron.edu

Garry Brown
Department of Mechanical and Aerospace Engineering
Princeton University
Princeton NJ 08544
glbao.3@outlook.com

ABSTRACT

Direct numerical simulations of a turbulent channel flow subject to an impulsive Reynolds number change are performed to obtain insights on late-stage transition as well as self-sustaining processes in turbulence. It is generally held that equilibrium in turbulent wall-bound flows is maintained by a balance between the outer and inner dynamics. This study aims to understand the role of the different components in achieving this balance by examining the nonequilibrium evolution caused by a forced imbalance between the inner and outer flow. The Reynolds number is increased or decreased by changing both viscosity and pressure gradient such that the mean vorticity at the wall remains unaltered at equilibrium. This provides a unique and ideal framework for understanding the path to the new equilibrium from a vorticity point of view. The results shows non-monotonic behavior that can be characterized into distinct phases. The near-wall vorticity field is observed to be the first to respond to the state change, followed by wall-shear stress and eventually the mean flow.

Introduction

There has been a great interest in understanding the equilibrium structures of fully developed wall-bound turbulence. Early direct numerical simulations (DNS) and experiments provided a statistical description of near-wall processes (Kim *et al.*, 1987), revealed the prevalence of streaks (Smith & Metzler, 1983) and provided insights on bursting events (Kim, 1985). Jiménez & Pinelli (1999) identified a near-wall cycle, involving quasi-streamwise vortices and near-wall streaks, as a part of a self sustaining process. It was argued that turbulence regeneration can persist while isolated from outer layer influences. Multiple models of turbulent regeneration have since been proposed (Jiménez, 2018).

Within the classical framework of boundary-layer theory, referring with scaling laws of viscous, buffer, and logarithmic layers, this near wall region is considered as both origin and key to turbulent equilibrium (Jiménez, 2013). Alternatively, high Reynolds-number studies demonstrate outer layer effects having a strong modulating influence on near wall turbulence through large-scale motion (Guala *et al.*, 2011).

Another significant challenge is the mechanistic understanding of the late-stage transition. Suryanarayanan *et al.* (2024) carried out DNS of a zero pressure gradient flat plate boundary layer undergoing classical transition by Tollmien–Schlichting waves and bypass transition by a distributed roughness strip. The late-stage mechanisms in both cases revealed that the eventual wall shear stress increase was caused by the emergence of near-wall streamwise vortices. The question of what causes the streamwise vortices to become dominant at a certain scale and distance away from the wall remains open. The dynamics of the near-wall streamwise vorticity is therefore key to understanding both transition to and self-sustaining mechanisms in equilibrium turbulent flows.

This paper thus seeks to provide additional insight into the dynamics of the near-wall streamwise vortices by examining the reactions of equilibrium turbulent channel flow when subjected to a non-physical scenario of instantaneously altered viscosity and pressure gradient. The motivation for doing so lies in the differing scales involved in channel flow structures (Schlichting & Gersten, 2016) allowing for investigation of each underlying process as the flow moves towards a new steady state. The nonequilbrium evolution is expected to remain homogeneous in the streamwise and spanwise directions and thus circumvents the additional challenge associated with strong streamwise dependence encountered in transition.

Previous studies into disruption of canonical flow via step change to pressure gradient by Seddighi *et al.* (2011) noted the existence of three stages of development - a delay stage, a responding stage, and a quasi-steady stage. This work differs in that the present scenarios vary both pressure gradient and viscosity such that the near wall time scale via $(d\overline{u}/dy)_w$ is the same between the original and the altered equilibrium states. This allows isolation of the reaction and relaxation periods as those departing and returning to the equilibrium state. In addition, the step change to viscosity has direct effects upon vorticity development. This may be demonstrated using the balance between vorticity dissipation and production terms. Using the enstrophy evolution equations in a flux-balance form Brown *et al.* (2015) yields the equation.

$$\iiint \left(\frac{d}{dt}\left(\frac{1}{2}{\omega_x}^2\right)\right) dV + \iint \left(u_j \frac{1}{2}\omega_x^2 - \nu \frac{\partial}{\partial x_j}\left(\frac{1}{2}\omega_x^2\right)\right) n_j dS = \underbrace{\iiint \left[\omega_x^2 \frac{\partial u}{\partial x} + \omega_x\omega_y \frac{\partial v}{\partial x} + \omega_x\omega_z \frac{\partial w}{\partial x}\right] dV}_{\text{production}} + \underbrace{\iiint \left[\nu\left(\left(\frac{\partial \omega_x}{\partial x}\right)^2 + \left(\frac{\partial \omega_x}{\partial y}\right)^2 + \left(\frac{\partial \omega_x}{\partial z}\right)^2\right)\right] dV}_{\text{dissipation}} \quad (1)$$

The production terms are expected to scale as $(u_{\text{vor}}/l_{\text{vor}})^3$, where u_{vor} and l_{vor} are velocity and length scales associated with near-wall vortices (that are expected to scale with u_τ and ν/u_τ *in equilibrium*). The dissipation terms scale as $\nu({u_{\text{vor}}}^2/{l_{\text{vor}}}^4)$, and are expected to be in balance with the production terms when the flow is at equilibrium. Note that in the present simulations, while viscosity and pressure gradient are impulsively changed, the velocity field itself does not undergo an instantaneous change, but rather evolves over time from its previous state. Therefore, at the moment viscosity is changed, u_{vor} and l_{vor} that depend on the velocity field, and by consequence the production terms in Eq.1, remain the same as the instant before the viscosity change. On the other hand, the dissipation terms that scale as $\nu({u_{\text{vor}}}^2/{l_{\text{vor}}}^4)$ are instantly altered. This leads to an imbalance between vorticity production and dissipation and drives the non-equilibrium evolution.

Possible insights this may bring into how equilibrium is maintained are analyzed from a vorticity point of view. An analysis of the evolution of mean velocity profiles of the flow through the Log and Defect laws is also conducted, though moderate Reynolds numbers are utilized.

Methodology

Direct Numerical Simulations (DNS) were performed using a pseudo spectral code based on the channel flow algorithm developed by Kim *et al.* (1987). This code was presented by Goldstein *et al.* (1993), and has been extensively used and validated in previous work (Strand & Goldstein, 2007; Goldstein *et al.*, 2017; Suryanarayanan *et al.*, 2024). Additionally, comparison of x-z and time averaged statistics to those of Kim *et al.* (1987) results in close agreement (Fig. 2). The domain is periodic in the streamwise and spanwise directions, with no-slip walls on the upper and lower boundaries. The y-normal plane is a uniform cartesian grid, while the y direction has a Chebyshev grid. The simulations presented in this paper use different resolutions depending on the range of $Re_\tau(= u_\tau\delta/\nu$, where δ is the half height of the channel), considered for each scenario. For scenarios involving an Re_τ of 360, a grid size (GI) of 576 by 192 by 288 is utilized for the streamwise (x), wall normal (y) and spanwise (z) directions. For those involving an Re_τ of 180 or lesser, a resolution of 384 by 128 by 192 (GII) is utilized. All grid sizes listed are of 3/2 de-aliased space. For spectral grid density in wall units, refer to table 1. The streamwise and spanwise extents of the domain are 6.28 H and 1.72 H respectively, where H is the total channel height.

Table 1. Grid Size in Wall Units

Grid	Re_τ	Δx^+	Δz^+	$min\Delta y^+$	$max\Delta y^+$
GI	180	5.89	2.94	0.048	5.89
GII	180	8.83	4.41	0.108	8.83
GI	360	11.78	5.88	0.096	11.8
GII	120	5.89	2.94	0.072	5.89

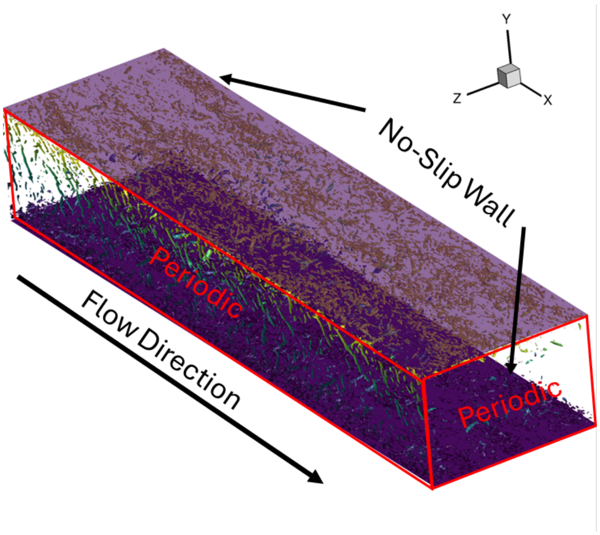

Figure 1. Depiction of Channel Flow Setup

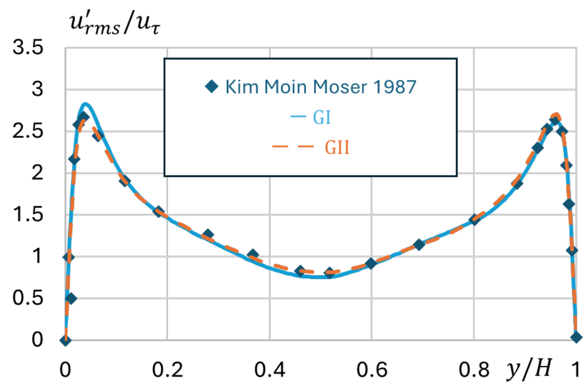

Figure 2. Validation of DNS

Three scenarios are considered. The first two simulations begin with an equilibrium turbulent channel flow at $Re_\tau = 180$. The viscosity is instantaneously changed at $t = 0$ such that Re_τ becomes 360 in the first scenario and 120 in the second scenario. The pressure gradient in these simulations is also changed at $t = 0$ to ensure that the *steady state* $d\overline{u}/dy|_{\text{wall}}$ remains unaltered by the viscosity change. Thus it may be expected that vorticity magnitudes should have steady state values similar to that seen before change in viscosity. The third scenario begins with an equilibrium turbulent channel flow at $Re_\tau = 360$ and undergoes a sudden change in viscosity and pressure gradient to reach $Re_\tau = 180$.

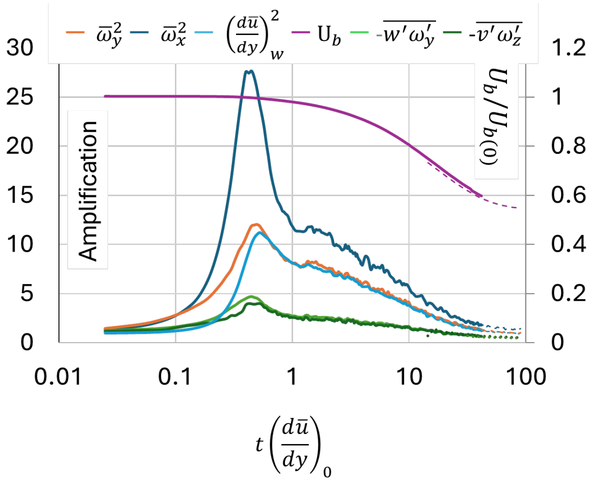

Figure 3. Temporal evolution of flow variables for the $Re_\tau = 180 \rightarrow 360$ case. Each variable is normalized by its value at $t = 0$ ($Re_\tau = 180$)

Results

Increasing Re_τ scenario

In the first scenario (Figs. 3 to 8), the evolution can characterized by three distinct phases.

In phase I, immediately following the drop in viscosity and pressure gradient there is a spike in both $\overline{\omega_x^2}$ and $\overline{\omega_y^2}$. The respective amplification of maximum magnitude is a factor of 27.7 and 12, with both values peaking at $0.45/(du/dy)_0$, where $(du/dy)_0$ is the average velocity gradient at the wall before the viscosity change. The present simulation therefore lacks the "delay stage" noted by Seddighi *et al.* (2011), likely due to differences in reaction between a purely pressure gradient step change and one undergoing a step change to both pressure gradient and viscosity, as noted by the analysis of Eq.1.

The Reynolds shear stress can be expressed in terms of vorticity fluxes as $\partial(-\overline{u'v'})/\partial y = \overline{v'\omega_z'} - \overline{w'\omega_y'}$ (Brown *et al.*, 2015; Suryanarayanan *et al.*, 2024). It can be seen that the peak values of both vorticity flux components rise along with streamwise vortex intensity. This is consistent with the argument that $-\overline{w'\omega_y'}$ has its origins in near-wall streamwise vortices (Suryanarayanan *et al.*, 2024). The increase in vorticity appears to originate at a few specific regions and spread outward in a manner not unlike nascent turbulent spots (Fig. 5). Note, however, these intense turbulent regions are not surrounded by laminar flow but by lower intensity turbulent flow (that was previously at equilibrium). The point of origin of these zones of increased turbulence overlaps with low speed and high speed streaks supporting their proposed origin in the breakdown of streaks. $d(\overline{u}/dy)^2|_{\text{wall}}$ increases by a factor of 11.2 and peaks at $t = 0.52/(du/dy)_0$. This is consistent with the wall shear stress increase by the counter gradient vorticity transport by $-\overline{w'\omega_y'}$ proposed by Suryanarayanan *et al.* (2024). The observed overshoot in vorticity in this phase is likely an indicator of vastly different time scales between vorticity production and mean kinetic energy dissipation.

Phase II ($t(du/dy)_0 \approx 0.5 - 1.5$) follows the maxima in the near-wall vorticity fields and is defined by the correction of the overshoot. The vorticity profiles at this stage remain distinct from the equilibrium profiles even when scaled with $d\overline{u}/dy$ at that time, as seen in Fig. 6.

Phase III ($t > 1.5/(du/dy)_0$) is characterized by a establishment of quasi-equilibrium and this can be observed to cause a distinct shift within the temporal progression of the

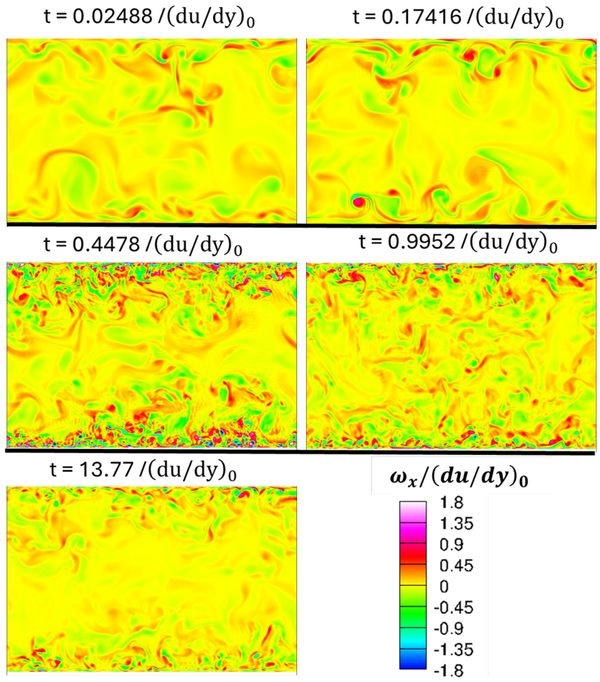

Figure 4. Evolution streamwise vorticity in $y-z$ planes for the $Re_\tau = 180 \rightarrow 360$ case

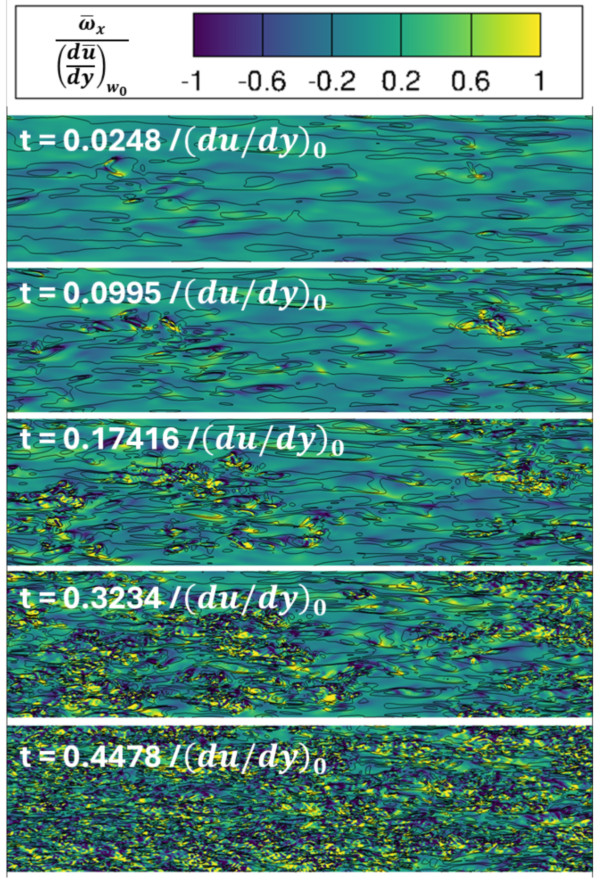

Figure 5. Evolution of streamwise vorticity in $x-z$ planes at $y/\delta = 0.01$ for the $Re_\tau = 180 \rightarrow 360$ case

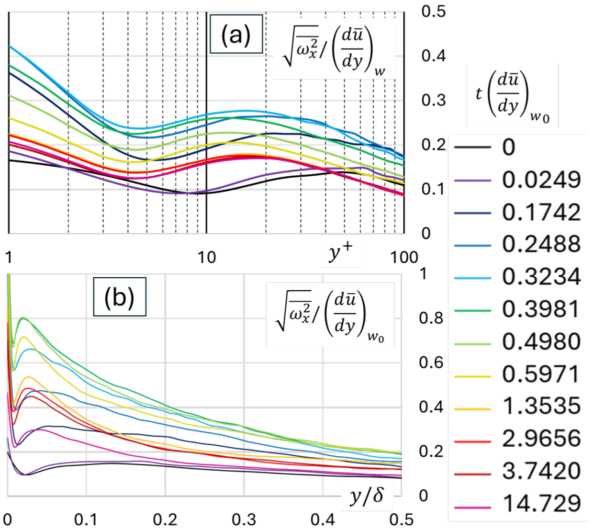

Figure 6. Evolution of $\frac{\sqrt{\omega_x^2}}{\frac{du}{dy}}$ profiles for the $Re_\tau = 180 \to 360$ case

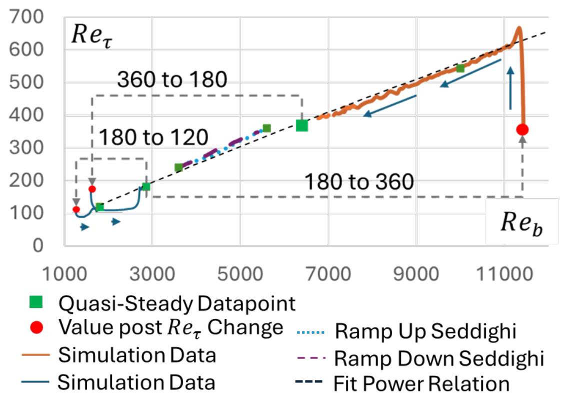

Figure 7. Re_τ as a function of Re_b

different statistics in Fig. 3. This is better observed from the vorticity profiles at different times (Fig. 6) which demonstrates convergence *when scaled by local wall vorticity* beyond $t = 2.96/(du/dy)_0$. This finding is further supported by examining the behavior of Re_τ as a function of Re_b (Fig. 7), where the relation passes through the equilibrium values for different Reynolds numbers. This phase therefore resembles stage III of Seddighi *et al.* (2011), who observed maintenance of quasi-equilibrium in evolving step-up and down simulations.

The location of vorticity production, typically found at $y^+ \approx 10.6$ (Schlichting & Gersten, 2016), is expected shift with the change to viscosity as the y^+ value associated with a given physical position adjusts instantaneously with the local viscous scaling, forcing a re-adjustment of the flow. The effect of instantaneously altered viscosity upon y^+ scaling may be observed by scaling the $\sqrt{\omega_x^2}$ profiles with the local wall vorticity at the respective time in Fig. 6. This can also be seen from the log law profile shown in Fig. 8B. It can be argued (Malkus, 2003) that this change in viscosity disrupts equilibrium by decreasing the smallest scale of vorticity transport.

We next consider the evolution of mean velocity profiles following the viscosity change. Seddighi *et al.* (2011) found that in their simulations following the abrupt change in pressure gradient, the mean velocity profiles at different times during the evolution continue to follow the log-law when scaled with the u_τ at the respective time. To explore if the present $Re_\tau 180 \to 360$ simulation shows a similar character, log-law is fit to the present data using the Ξ method as devised by Österlund *et al.* (2000).

It must be emphasized that due to the modest Reynolds numbers considered, the results on the mean velocity profile need to be interpreted with caution. The results indicate that the law of the wall being near-instantaneously disrupted by the change to ν. Manual fitting of log law (Krug *et al.*, 2017; Österlund *et al.*, 2000) (not shown here) indicated approximate maintenance of near log profiles before (Phase I) and after the vorticity peak (Phase II), albeit with a different κ. One has to be careful interpreting this change to κ - it does not necessarily indicate a systematic variation in the Karman constant, but is a consequence of sudden ν change. At the instant of the viscosity change, this can be readily shown to be $\kappa_2 = \kappa_1\sqrt{\nu_2/\nu_1}$.

In the quasi-equilibrium Phase III the velocity profiles appear to collapse when scaled with wall variables and approach the canonical log-law.

Defect law examination (Fig. 8A) indicates large-scale departure from equilibrium between $y/\delta \approx 0.01$ to 0.1 at t = $0.323/(du/dy)_0$ and $0.398/(du/dy)_0$ during the vorticity spike (phase I). The sharper profiles near the wall are consistent with increased $\overline{\omega_x^2}$ levels. Fitting of the wake equation (Coles, 1956) with the wake function presented by Coles (1968) demonstrates the earlier stated variation in κ, as well as variation in Π. The near wall defect returns to equilibrium levels coinciding with the vorticity peak at $0.438/(du/dy)_0$ at the end of phase I.

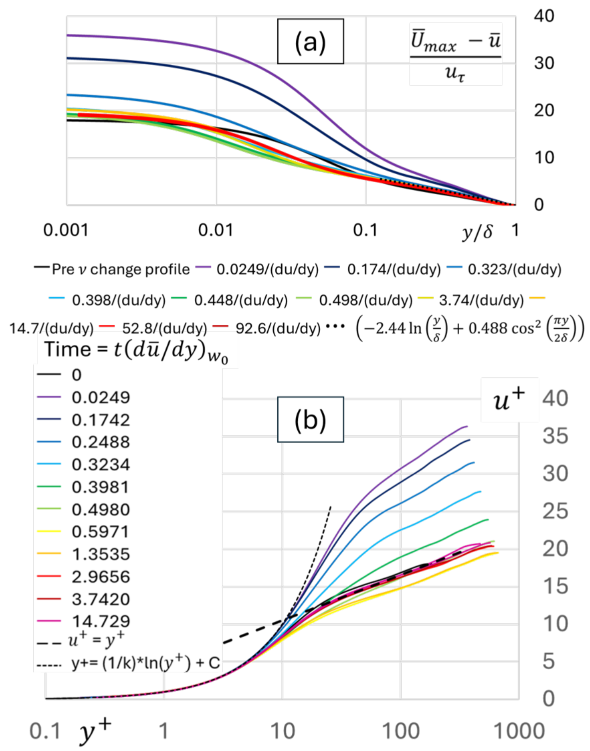

Figure 8. Evolution of Defect Law (A) and Log Law (B) profiles the $Re_\tau = 180 \to 360$ case

The concurrence of the return of equilibrium κ with the peak in vorticity in the specific scenario considered here raises the question of whether there is an underlying relation that

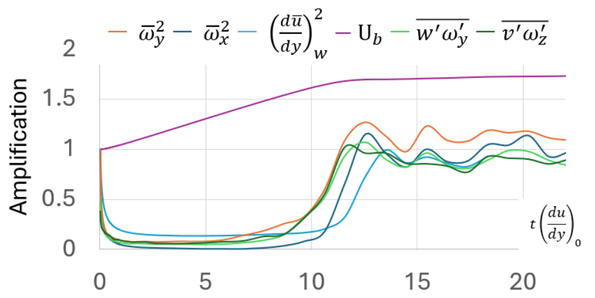

Figure 9. Temporal evolution of flow variables for the $Re_\tau = 360 \rightarrow 180$ case. Each variable is normalized by its value at $t = 0$ ($Re_\tau = 360$)

needs to be examined. The synchronization of the equilibration of u_{max}/u_τ with the vorticity maxima (Fig. 8A) suggests that the first step of reestablishing equilibrium may involve correcting the velocity scale deficit between inner and outer flows, and that vorticity transport plays a key role in achieving this balance.

Decreasing Re_τ scenarios

The decreasing Re_τ scenarios show a distinctly different behavior. For the scenario of decreasing Re_τ from 360 to 180 (Fig. 9), the instantaneous ν alteration initiates a 99.8% decrease in $\overline{\omega_x^2}$, 96.0% decrease in $\overline{\omega_y^2}$, and an 89.8% decrease in $(d\bar{u}/dy|_w)^2$, with minimum values reached at $t(du/dy)_0 = 4.97$, 2.71, and 1.35 respectively. This sudden drop in $(d\bar{u}/dy|_w)^2$ following $\overline{\omega_x^2}$ is due to the loss of the countergradient transport mechanisms and is consistent with the proposal of Suryanarayanan *et al.* (2024), and also follows logically from the analysis of the enstrophy equations conducted earlier. The near uniform acceleration during the reduced vorticity period indicates a close to laminar flow, which is consistent with observations by Jiménez & Pinelli (1999) that relaminarization may be induced via suppressing even a single turbulence regeneration component. This laminar-esque state occurs despite the targeted Re_τ expected to be turbulent. Observation of effective Re_τ shows a significant decrease below 180 due to the drop in $(d\bar{u}/dy|_w)$ during the nonequilibrium relaxation. Unlike the increasing Re_τ case, there exists no point at which Re_b possesses a relation with Re_τ indicative of a quasi-steady state, signifying a different route to equilibrium (Fig. 7).

Note that the ratio of $\overline{\omega_x^2}/\overline{\omega_y^2}$ drops by an order of magnitude between $t(du/dy)_0 = 0$ to 6.73, indicating that the reduction in $\overline{\omega_x^2}$ is more severe than $\overline{\omega_y^2}$. This relates to the association of $\overline{\omega_y^2}$ with streaks, which being larger structures resist additional viscous dissipation when compared to $\overline{\omega_x^2}$, which contains finer-scale hairpin vortices. This implies that within the bounds of this simulation, $\overline{\omega_y^2}$ serves as a seed variable that survives the 'viscosity-jump extinction' event and leads the turbulent recovery.

One could ask the question if the quasi-relaminarization observed in Fig.9 could be attributed to an drop in Re_τ below a critical value (ie, once$(d\bar{u}/dy|_w)$ is sufficiently low, Re_τ is too low to sustain turbulence). This view is however challenged by the results shown in Fig. 10. When Re_τ decreases from 180 to 120, it experiences a 95.5% decrease in $\overline{\omega_x^2}$ (minimum value reached at $t(du/dy)_0 = 2.41$), while reaching a lower effective Re_τ than the previous scenario (minimum Re_τ = 89.8 vs 108). This finding leads to the conclusion that the relaminarization

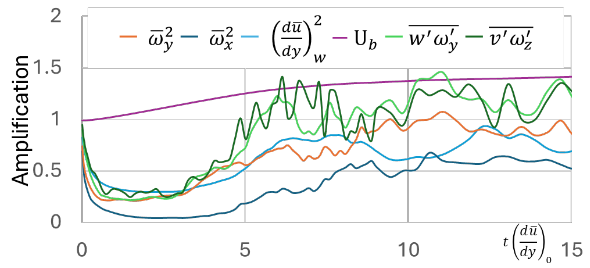

Figure 10. Temporal evolution of flow variables for the $Re_\tau = 180 \rightarrow 120$ case. Each variable is normalized by its value at $t = 0$ ($Re_\tau = 180$)

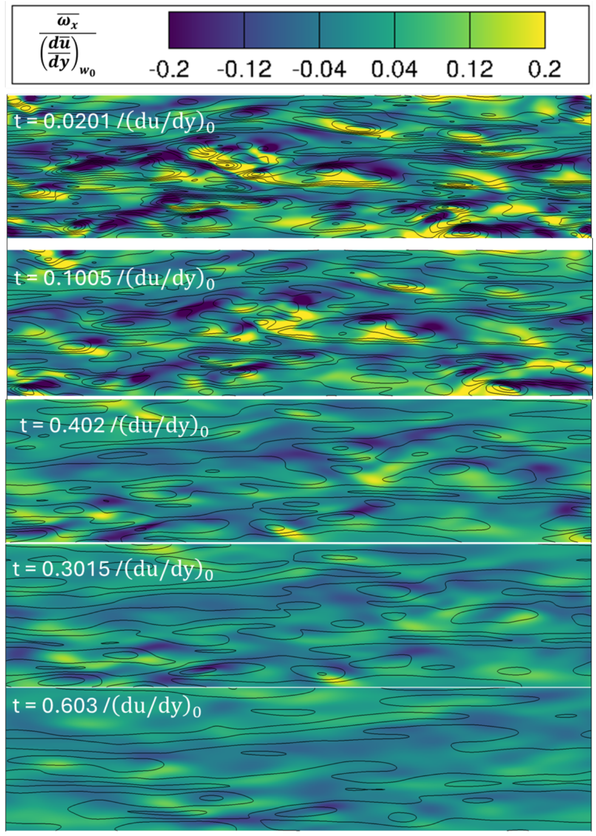

Figure 11. x-z plane at $y/\delta = 0.01$ demonstrating dissipation over time of near wall ω_x normalized by $(d\bar{u}/dy|_w)$ with isolines of streamwise velocity

effects noted in Fig. 9 is a result of severe imbalance between production and dissipation terms caused by the sudden viscosity change and not merely a function of Reynolds number dropping below a critical value. Additionally, an 79.6% decrease in $\overline{\omega_y^2}$, and an 70.5% decrease in $(d\bar{u}/dy|_w)^2$ are observed, with minimum values reached at $t(du/dy)_0 = 2.09$ and 1.77 respectively. The more rapid recovery of $\overline{\omega_y^2}$ supports the idea that it serves as a seed variable. Curiously the vorticity flux terms contributing to Reynolds stress, $w'\omega_y'$ and $v'\omega_z'$, experience a lesser suppression than $\overline{\omega_x^2}$, both values experiencing a reduction on a similar order to that of $\overline{\omega_y^2}$. The dissipation of ω_x near the wall is depicted in Fig. 11, where the decreasing density of velocity isolines demonstrates the associated reduction in near wall flow mixing.

Concluding Remarks

The present results lead to the following preliminary conclusions:

1. $\overline{\omega_x^2}$ consistently reacts to flow alterations more rapidly than any other observed variable. This may be seen in the increasing Re_τ scenario, where the spike in vorticity precedes changes to even near wall velocity profile, which is almost entirely dependent upon viscosity shear. The timescales involved in its increase and overshoot indicate a degree of timescale separation between vorticity production, velocity profile alteration, and bulk flow acceleration or deceleration.

2. Profiles of Re_τ as a function of Re_b demonstrate that there are significant differences caused by performing a step change to both viscosity and pressure gradient rather than to only pressure gradient as in the work of Seddighi *et al.* (2011). This is a result of viscosity directly effecting the balance between vorticity production and dissipation terms. This being said, the relaxation phase (III) of the increasing Re_τ scenario corroborates the findings of Seddighi *et al.* (2011) regarding quasi-equilibrium states.

3. For the decreasing Re_τ scenario, the same separation of scales may be seen in both the apparent relaminarization of flow and in its recovery, where once again any change to velocity profile is preceded by changes to vorticity. This implies that for non-equilibrium flows such as those examined by this paper, the rapid response of smaller scale terms such as vorticity to changes in the flow allows them greater influence . Comparative reduction and time of recovery support the near wall cycle concept for turbulent regeneration (Jiménez & Pinelli, 1999). These results also suggest near wall turbulence may be re-initiated by a single component of that cycle.

Additionally, the broad insights obtained from the simulations and analyses carried out in this paper suggest that disruption, emergence and sustainment of equilibrium in wall-bound turbulence can be explained from a vorticity point of view. This leads us to contemplate if vorticity dynamics is central to the law of the wall, and more generally, to the nature of equilibrium turbulence itself.

Acknowledgments

The authors would like to thank Prof. David Goldstein (The University of Texas at Austin) for discussions on this topic, and the Ohio Supercomputer Center for computational resources.

REFERENCES

Brown, Garry L, Lee, Myoungkyu & Moser, Robert D 2015 Vorticity transport: the transfer of viscous stress to reynolds stress in turbulent channel flow. In *Ninth International Symposium on Turbulence and Shear Flow Phenomena*. Begel House Inc.

Coles, Donald 1956 The law of the wake in the turbulent boundary layer. *Journal of Fluid Mechanics* **1** (2), 191–226.

Coles, Donald 1968 The young person's guide to the data .

Goldstein, David, Chu, Jeff & Brown, Garry 2017 Lateral spreading mechanism of a turbulent spot and a turbulent wedge. *Flow, Turbulence and Combustion* **98** (1), 21–35.

Goldstein, D, Handler, R & Sirovich, L 1993 Modeling a no-slip flow boundary with an external force field. *Journal of computational physics* **105** (2), 354–366.

Guala, Michele, Metzger, M & McKeon, Beverley J 2011 Interactions within the turbulent boundary layer at high reynolds number. *Journal of Fluid Mechanics* **666**, 573–604.

Jiménez, Javier 2013 Near-wall turbulence. *Physics of Fluids* **25** (10).

Jiménez, Javier 2018 Coherent structures in wall-bounded turbulence. *Journal of Fluid Mechanics* **842**, P1.

Jiménez, Javier & Pinelli, Alfredo 1999 The autonomous cycle of near-wall turbulence. *Journal of Fluid Mechanics* **389**, 335–359.

Kim, John 1985 Turbulence structures associated with the bursting event. *The Physics of fluids* **28** (1), 52–58.

Kim, John, Moin, Parviz & Moser, Robert 1987 Turbulence statistics in fully developed channel flow at low reynolds number. *Journal of fluid mechanics* **177**, 133–166.

Krug, Dominik, Philip, Jimmy & Marusic, Ivan 2017 Revisiting the law of the wake in wall turbulence. *Journal of Fluid Mechanics* **811**, 421–435.

Malkus, Willem VR 2003 Borders of disorder: in turbulent channel flow. *Journal of Fluid Mechanics* **489**, 185–198.

Österlund, Jens M, Johansson, Arne V, Nagib, Hassan M & Hites, Michael H 2000 A note on the overlap region in turbulent boundary layers. *Physics of Fluids* **12** (1), 1–4.

Schlichting, Hermann & Gersten, Klaus 2016 *Boundary-layer theory*. springer.

Seddighi, Mehdi, He, Shuisheng, Orlandi, Paolo & Vardy, Alan E 2011 A comparative study of turbulence in ramp-up and ramp-down unsteady flows. *Flow, turbulence and combustion* **86** (3), 439–454.

Smith, CR & Metzler, SP 1983 The characteristics of low-speed streaks in the near-wall region of a turbulent boundary layer. *Journal of Fluid Mechanics* **129**, 27–54.

Strand, James Stephen & Goldstein, D 2007 Dns of surface textures to control the growth of turbulent spots. PhD thesis, University of Texas at Austin.

Suryanarayanan, Saikishan, Goldstein, David B & Brown, Garry L 2024 Late-stage boundary layer transition mechanisms: A vorticity point of view. *Physics of Fluids* **36** (8).